Geofísica Internacional (1991) Vol. 30, Num. 3, pp. 121-134

Remote and local forcing of Rossby wave variability in the midlatitude Pacific Ocean

A. Parés-Sierra
Scripps Institution of Oceanography, La Jolla, Calif., U. S. A. and
Centro de Investigación y Estudios Superiores de Ensenada, Ensenada, B. C., México

Received: 12 February, 1991; Accepted: 14 August, 1991.

RESUMEN

Un modelo de gravedad reducida se utilizó para investigar la variabilidad de baja frecuencia en el Pacífico Nororiental. El dominio del modelo abarca desde los 18°N hasta los 50°N y desde 155°O hasta la costa oeste de Norteamérica. En un primer experimento, el modelo es forzado por el esfuerzo del viento (COADS). Un segundo experimento consiste en forzar el modelo a través de su frontera austral usando los resultados de un modelo ecuatorial de gravedad reducida. Encontramos que los espectros de número de onda-frecuencia calculados a partir de los resultados de nuestro modelo son congruentes con los calculados a partir de observaciones. La mayor parte de la energía de baja frecuencia en el interior del océano modelado consiste en ondas de Rossby propagándose hacia el oeste. El análisis de la respuesta del modelo a los dos forzamientos (forzamiento local por el viento y forzamiento remoto a través de la frontera) nos muestra que ambos mecanismos son capaces de generar el tipo de ondas que determina la variabilidad en el interior del océano. En los resultados del modelo forzado por el viento se observa la existencia de una latitud crítica alrededor de los 35° N. La respuesta del modelo al norte y sur de esta latitud es marcadamente diferente, principalmente en cuanto a las características de propagación de las ondas predominantes: se observa un fuerte componente de decaimiento al norte y de propagación al sur de dicha latitud.

PALABRAS CLAVE: Ondas de Rossby, latitud crítica.

ABSTRACT

A reduced-gravity model is used to investigate the low-frequency variability in the eastern mid-latitude Pacific Ocean. The domain covers the eastern North Pacific from 18°N to 50°N and from 155°W to the North American coast. In a first experiment the model is forced by the wind stress from COADS. A second experiment consists in forcing the model from its southern boundary using the results of an equatorial reduced-gravity model. The wavenumber-frequency spectrum calculated from the model is consistent with observations. Most of the calculated low-frequency variability in the ocean interior is in the form of westward propagating Rossby waves. Investigation in the wavenumber-frequency domain shows that either mechanism (locally wind-forced and remotely forced coastal disturbances) is capable of generating the westward-traveling waves that determine the ocean interior variability. For the locally forced model a critical latitude at about 35°N is observed. The disturbances in the region north and south of this latitude present a clear dichotomy in their propagating characteristics: a strong off-shore decaying factor to the north and off-shore propagation to the south.

KEY WORDS: Rossby Waves, Critical latitude.

INTRODUCTION

Most of the mesoscale variability of the midlatitude Pacific Ocean is associated with long baroclinic Rossby waves (Emery and Magaard, 1976; Price and Magaard, 1980; White and Saur, 1981). Several studies have addressed the generation of annual and interannual Rossby waves in the Pacific. White and Saur (1981, 1983) investigated the source of this variability in the thermal structure of the eastern subtropical North Pacific. For interannual periods they identified the sea level variability along the eastern boundary as the dominant source mechanism south of 30°N and a wind-driven mechanism north of 30°N. They also investigated the resonant response of the interannual baroclinic Rossby waves to wind forcing and found that, for some regions, a model implementing this mechanism could simulate 60 to 90% of the mesoscale variability.

The annual variation of the curl of the wind has also been identified as a source of annual Rossby waves in the North Pacific (e.g. Cummins *et al.*, 1986; White and Tabata, 1987). By using a quasigeostrophic model in their analysis, however, Cummins *et al.* (1986) eliminated one possibly important coastal generating mechanism of Rossby waves, namely northward traveling Kelvin waves along the eastern boundary. McCreary (1976) suggested the possibility of Kelvin waves being a source of Rossby wave activity. Using a model that incorporates ageostrophic internal Kelvin waves to satisfy the eastern boundary condition, Mc Creary (1976) allowed for the generation of westward propagating baroclinic long waves in the wake of the former. Cane and Sarachik (1977) give a good explanation of this process.

Parés-Sierra and O'Brien (1989) hereafter referred to as PO) demonstrated the importance of the equatorially generated variability in the coastal eastern Pacific region. They showed that most of the interannual variability, and an important percentage of the annual and semiannual variability, can be accounted for by the effect of variability generated at the equator and propagated poleward in the form of coastally trapped Kelvin waves. This paper investigates the leakage of this energy to the ocean interior.

The paper is organized as follows: in the second section we briefly present the models used and the way the data for the analysis were extracted. The third and fourth sections present the results and discussion while in the last section a summary is given and the conclusions are stated.

MODEL AND DATA

A reduced-gravity model which incorporates the realistic geometry of western North America was used in this study (see PO for details). The equations of the model are:

$$\frac{\partial U}{\partial t}+\frac{1}{a\cos\theta}\frac{\partial}{\partial\phi}\left(\frac{U^2}{H}\right)+\frac{1}{a}\frac{\partial}{\partial\theta}\left(\frac{UV}{H}\right)-(2\Omega\sin\theta)V=$$

$$\frac{-g'}{2a\cos\theta}\frac{\partial H^2}{\partial\phi}+\frac{\tau^{\phi}}{\rho}+A\nabla^2 U,$$

$$\frac{\partial V}{\partial t}+\frac{1}{a\cos\theta}\frac{\partial}{\partial\phi}\left(\frac{UV}{H}\right)+\frac{1}{a}\frac{\partial}{\partial\theta}\left(\frac{V^2}{H}\right)+(2\Omega\sin\theta)U=$$

$$\frac{-g'}{2a}\frac{\partial H^2}{\partial\theta}+\frac{\tau^{\theta}}{\rho}+A\nabla^2 V,$$

$$\frac{\partial H}{\partial t}+\frac{1}{a\cos\theta}\left[\frac{\partial U}{\partial\phi}+\frac{\partial}{\partial\theta}(V\cos\theta)\right]=0,$$

where θ and ϕ are the latitude and longitude; U and V are the transports in the east-west and north-south directions; H is the depth of the upper layer; g' the reduced-gravity; τ^{θ} and τ^{ϕ} the wind stresses components in the θ and ϕ directions, respectively; A an eddy viscosity coefficient and a the radius of the earth.

The model's domain is shown in Figure 1. Three experiments were performed: first the model was run using 19 years of wind stress data from the Comprehensive Ocean-Atmosphere Data Set (COADS); this is the local, or wind-forced model experiment. In order to include the variability generated below the southern boundary of our model (18°N), a second experiment was done in which the model was forced through its southern boundary by imposing the results of a wind-forced, reduced-gravity equatorial model (Kubota and O'Brien, 1987, Figure 1). Kubota and O'Brien's model includes the equatorial Pacific from 20°S to 20°N and was run initially from January 1961 through December 1984. Values of the transport (U, V) and upper layer thickness (ULT) were taken from this model along a band of 15 degrees of longitude from the American coast, at 18°N, every 6 days. A third experiment was done where both forcings were used simultaneously (local + remote). In all three experiments the period covered is from January 1961 to December 1979. The output of the model was sampled at points along the coast and at four latitude bands (at 24°, 33°, 38° and 43°N). Parés-Sierra and O'Brien (1989) report the results of the along-the-coast analysis, while this paper concentrates on the analysis of the relaxation of the coastal variability and its propagation to the ocean interior.

RESULTS

Mean and annual cycle

Several aspects of the steady large-scale circulation are reproduced by the model. Away from the coast, the basic mean state is determined by the large-scale negative wind-curl. The mean flow in the model is in Sverdrup balance. Figure 2 shows the 19-year long-term mean upper layer thickness (ULT). The dominant wind-curl driving mechanism is evident in this Figure. The deepest ULT occurs west of 140°W and from 20 to 35°N where the curl of the wind is more negative. The ULT decreases to the east and north of this region creating an east-west pressure gradient south of about 45°N, and east of 140°W. West of 140°W and north of about 25°N there is a general north-south pressure gradient. This pressure gradient pattern geostrophically drives the main gyre (i.e., the North Pacific Gyre) in our model.

The main seasonal variation along the coast is given by the upwelling and downwelling events, and the accompanying geostrophically adjusted poleward and equatorward coastal currents. This activity is directly driven by the strong seasonal reversal of the wind in the region (see PO). Along the coast, the winds are normally strong and are directed equatorward in spring-summer and poleward in fall-winter (Nelson, 1977). This seasonal wind variation drives most of the seasonal variability in the local model. During spring, a strong upwelling condition develops along the coast which in turn creates a negative pressure gradient that geostrophically drives an equatorward current. During fall and winter the winds weaken and may reverse direction, becoming southerly at some latitudes (Nelson, 1977); the upwelling ceases and eventually downwelling occurs generating a positive pressure gradient and the interior countercurrent or Davidson current. A complete analysis and description of the seasonal variability of the model results is found in PO; for the California Current System in general, see Hickey (1979), and, more recently, Lynn and Simpson (1988).

For the remote model, upwelling and downwelling events enter the domain through its southern boundary and propagate quickly poleward along the coast in the form of coastally trapped Kelvin waves. Figure 3 shows an 18-day

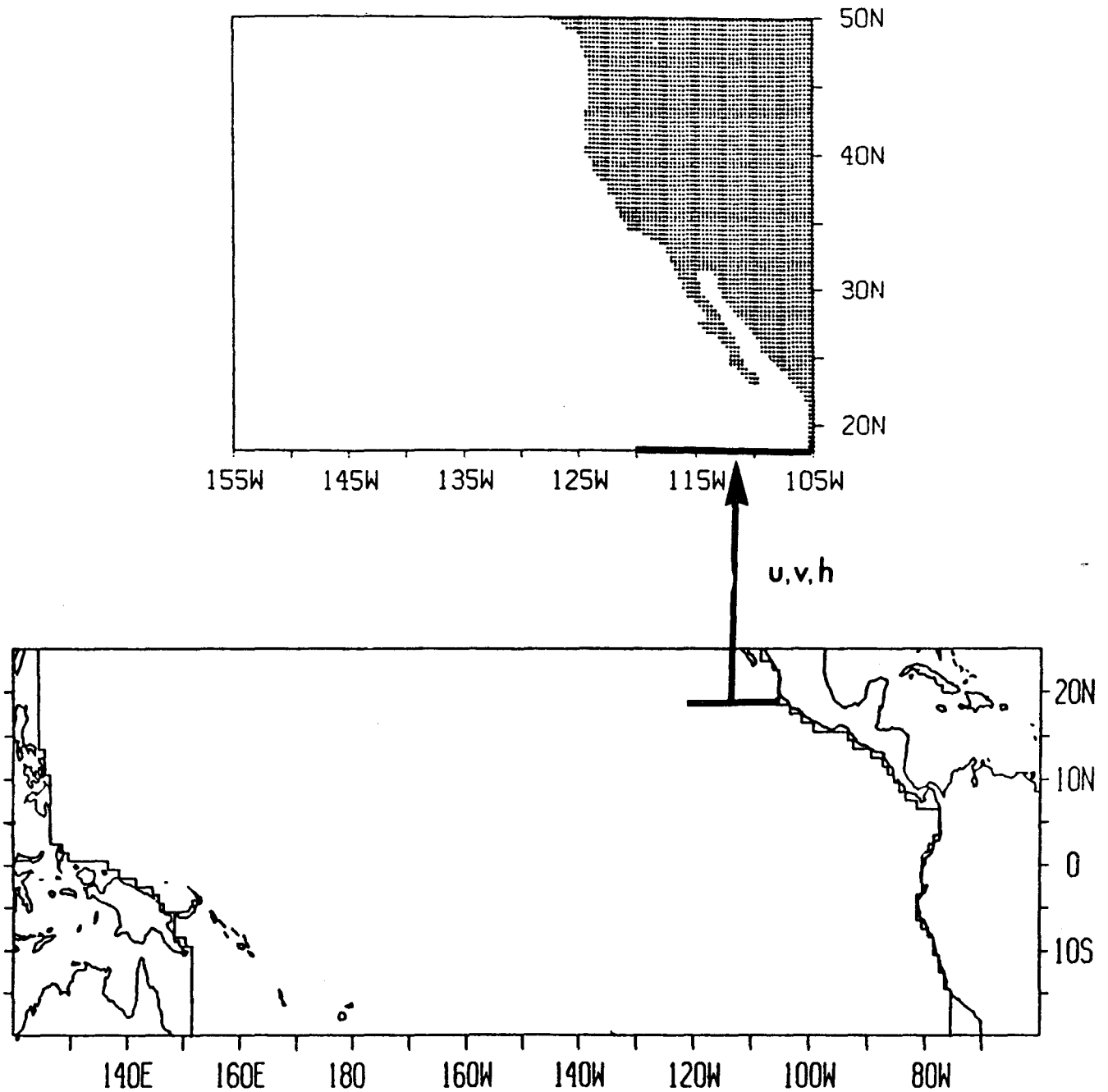

Fig. 1. Top: Model domain. The western, northern and southern boundaries are open. Bottom: Domain of the Kubota and O'Brien (1988) equatorial model used to force the remote model. U, V, and H values were taken from a 15 degrees transect at 18°N and imposed on our southern boundary (heavy line).

sequence (with 6 day interval) of ULT fields from the remote model. An upwelling event enters the domain in January 15, propagates north and, by February 3, its trailing edge reaches approximately 50°N.

To quantitatively assess the contributions of the locally and remotely forced variability to the total coastal energy, spectral analysis was performed on the ULT time series formed by sampling the results at four stations: Neah Bay, Crescent City, San Francisco, and San Diego. The spectra of sea level data for the same four stations were also calculated. It was shown (see PO) that for the local model the dominant period is the annual one at all stations, with a smaller but significant peak at the semiannual period. The background spectrum is red. Only at the annual period are the spectra from the local and remote models of comparable magnitude (Figure 4 shows the spectra for Crescent City, 42°N). In the remote model, the energy at the semiannual, annual and the 2-4 cycle/year frequency band are of similar magnitude. The background energy in the remote model

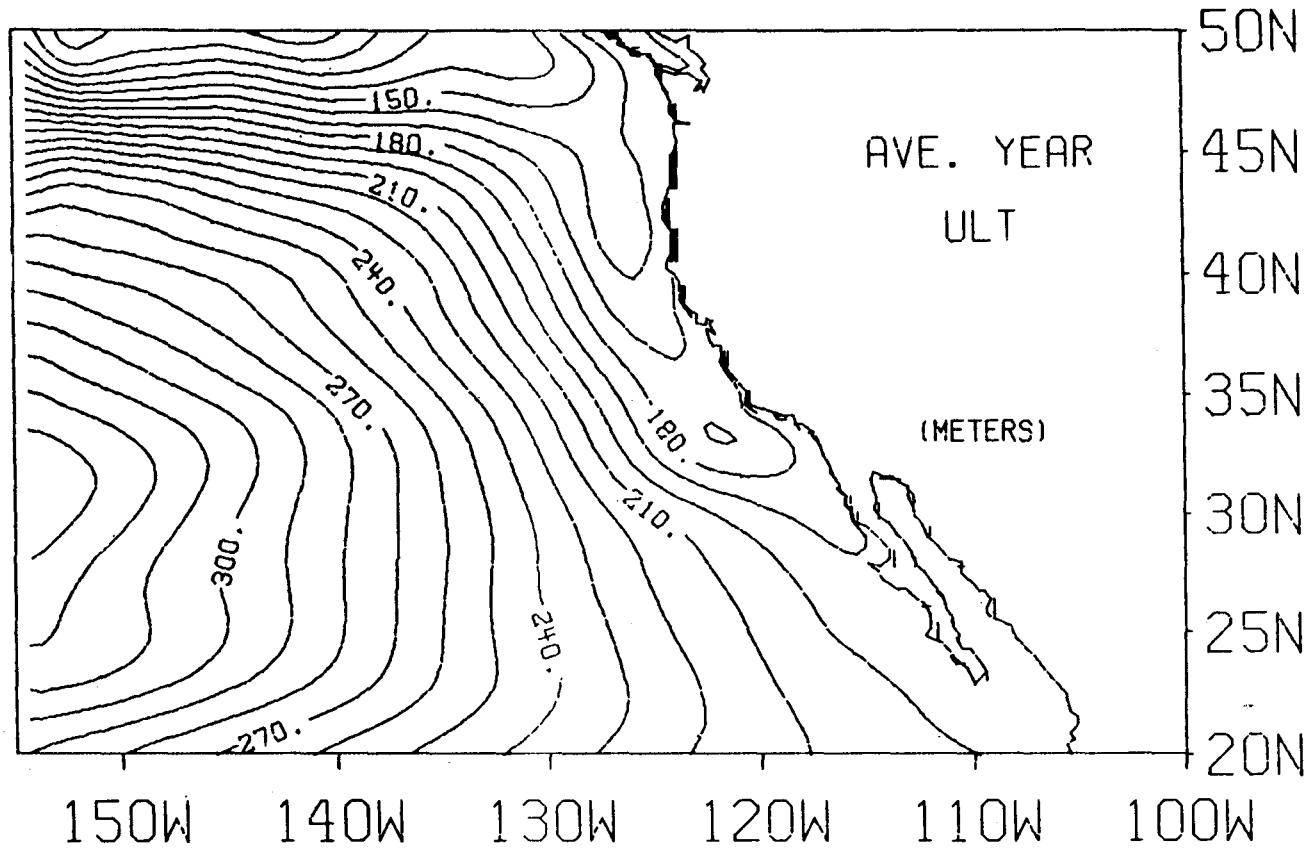

Fig. 2. Long term averaged ULT (meter) from the local wind-forced model. Contour interval is 10 m.

increases toward the low frequencies, but the amplitude is at least one order of magnitude greater than in the local model. This magnitude difference results in the local + remote model spectra being dominated by the remote model, except at the annual frequency. The spectrum variation with latitude is mainly for the magnitude of the annual peak. As shown in PO, the magnitude of the annual peak in the local + remote model increases to the north due to an increased energy at the annual period of the local wind-driven mode. By cross-spectral analysis between model results and observations at different stations along the coast, it was concluded that, at the coast, most of the interannual variability is of equatorial origin, while both locally and remotely forced variability contributed similarly to the seasonal and higher frequencies.

Westward propagation of perturbations

In our model both mechanisms (local and remote) generate westward propagating waves. For the local model, the long term ULT averaged monthly anomalies (Figure 5) show how the seasonal variation of the coastal anomalies relaxes by propagating westward. Positive anomalies in Figure 5 (pycnocline deeper than the 19-year mean) occur along the coast from October to February, while negative anomalies occur from March to August. The largest negative anomaly occurs in June, concurrently with the strongest equatorward wind near the coast. Figure 5 clearly shows that the relaxation of this seasonal variation is not in the form of a standing wave at the coast, but rather as a westward relaxation of the disturbance. Two regions appear to be the dominant sources of Rossby wave activity: from 20 to 25°N (presumably related to effect of the Gulf of California), and around 45°N where the strong wind reversal drives the strongest seasonal pattern of upwelling and downwelling. These two regions have been identified by Cummins *et al.* (1986) and by White and Saur (1981) as important sources of Rossby waves. Figure 5 also shows the existence of a critical latitude at about 35°N. It marks the line where the assumed plane wave solution changes character from off-shore propagating to off-shore decaying (eqs. 1 and 3 in the fourth section). South of 35°N the waves from the coast can propagate off-shore while to the north they present a strong offshore decaying component (McCreary and Kundu, 1985; McCreary *et al.*, 1987). The theoretical critical latitude for coastal trapping of an annual period wave in a north-south coast is farther north than 35°N (eq. 3); but as shown by Grimshaw and Allen (1988), the effect of the coastal inclination is pulling the critical latitude southward.

For the remote model a similar situation exists. The anomalies (this time not caused by a wind forced mechanism but propagated in the form of coastal Kelvin waves) leave the coast and propagate westward. The time scales of the two phenomena are very different: while the coastal

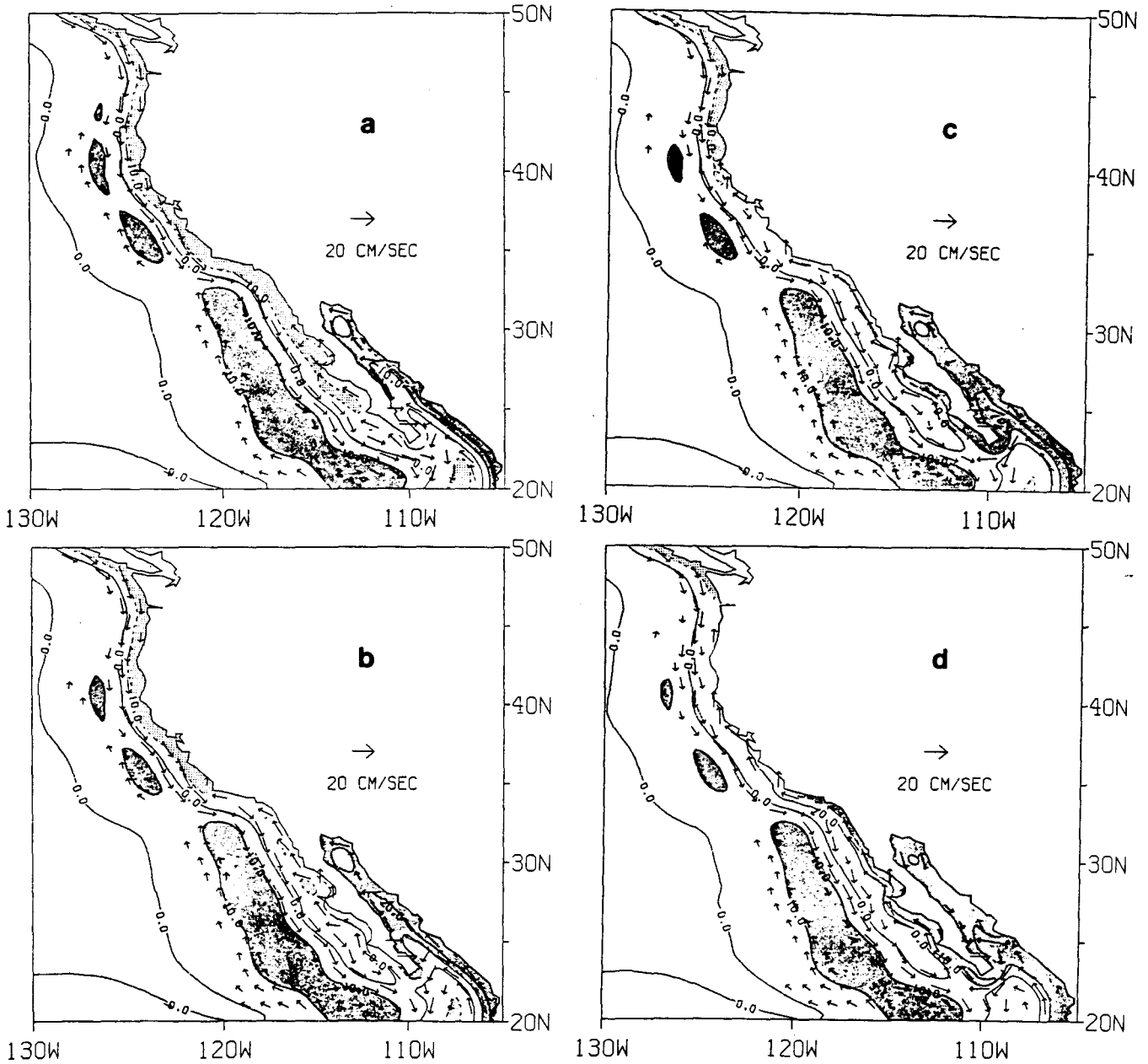

Fig. 3. Upper layer thickness anomaly (contours) and velocity (arrows) from the remotely forced model. Figure shows four snapshots of the results six days apart: a) January 15, b) January 21, c) January 27, and d) February 3. Scale of arrows as shown in the figure. ULT deeper than 10 m are dark-shaded and shallower than -10 m light-shaded.

Kelvin wave transmits the energy from south to north in a time scale of days, Rossby waves propagate westward at a much slower speed. From the point of view of the latter, the anomalies develop almost simultaneously all along the coast.

Figures 6a and 6b show two representative results from the remotely forced model. Both are snapshots of ULT anomalies for February 9; Figure 6a is for 1968 and 6b for 1975. The pattern is very similar: meridional bands of positive and negative anomalies extending over the whole domain with magnitude decreasing to the north and west. In both figures, there is a large positive anomaly close to the center of the domain that corresponds to the El Niño events occurring at the coast in 1965 and 1972. The different speed of propagation with latitude is evidenced by the sloping of the latitudinal bands. In Figure 6a, a strong negative anomaly is observed at about 120 - 130°W; this corresponds to the strong downwelling events (anti-El Niño) occurring at the coast in 1973. The weak positive contour in the western region, starting at the western boundary at 30°N and 40°N in both figures, corresponds to anomalies that were at the coast in 1963 and 1964 respectively. Recall that *all* the information in Figure 6 comes from a

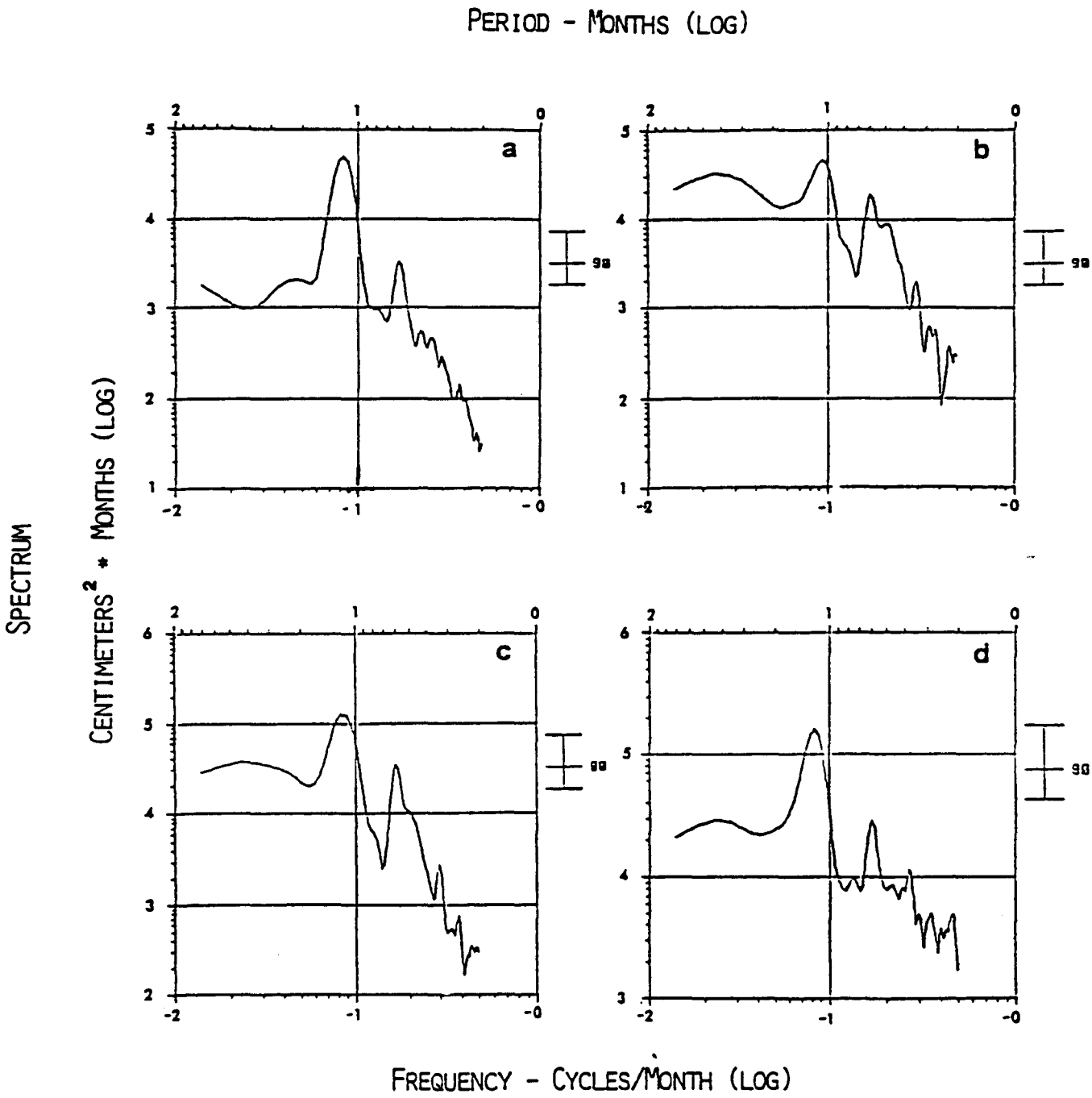

Fig. 4. Crescent City sea level spectra from (a) local model, (b) remote model, (c) local + remote model and (d) observations. Different scales were used for each spectrum. The 90% confidence intervals are shown to the right of each spectrum.

very small portion of the southern boundary of the domain; the implication of this will be discussed below.

DISCUSSION

White (1985) distinguished two sources of the generation of long baroclinic Rossby waves in the mid-Pacific Ocean: (1) Due to Ekman pumping by the wind stress curl and (2) Due to eastern boundary influence induced either locally or associated with remotely forced variability.

Mysak (1983) proposed a mechanism by which the north-south fluctuation of the Eastern Boundary Current off Vancouver Island can efficiently generate first baroclinic mode Rossby waves throughout the central Pacific. White and Saur (1981) used subsurface temperatures and surface salinity observations along the great circle transect between

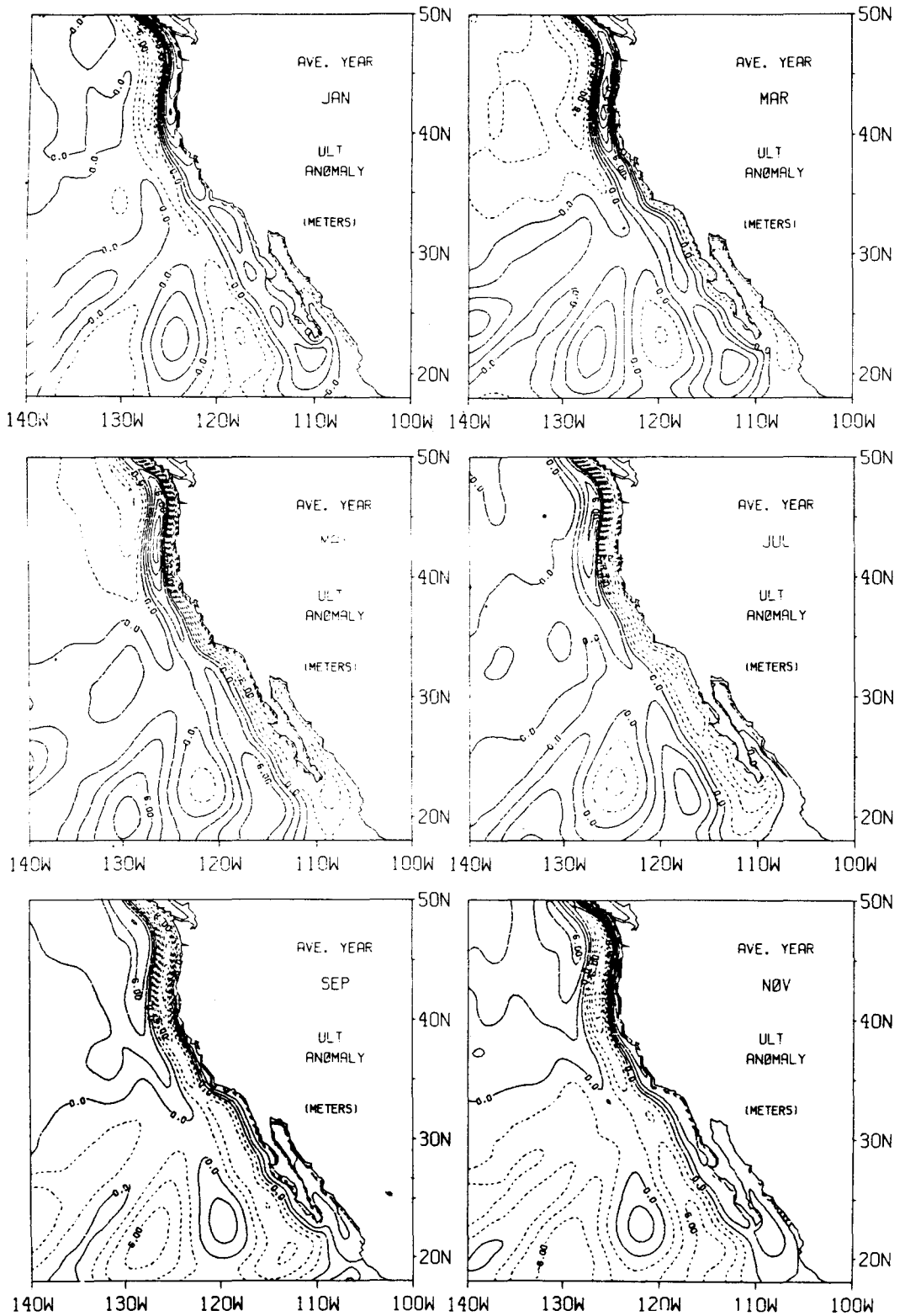

Fig. 5. Long-term monthly ULT anomaly from the local model. The long-term average was subtracted from the long-term monthly mean. Contour interval is 2 m. Strongest anomalies are generated near 40°N and from the mouth of the Gulf of California. Note the westward propagation of anomalies throughout the year.

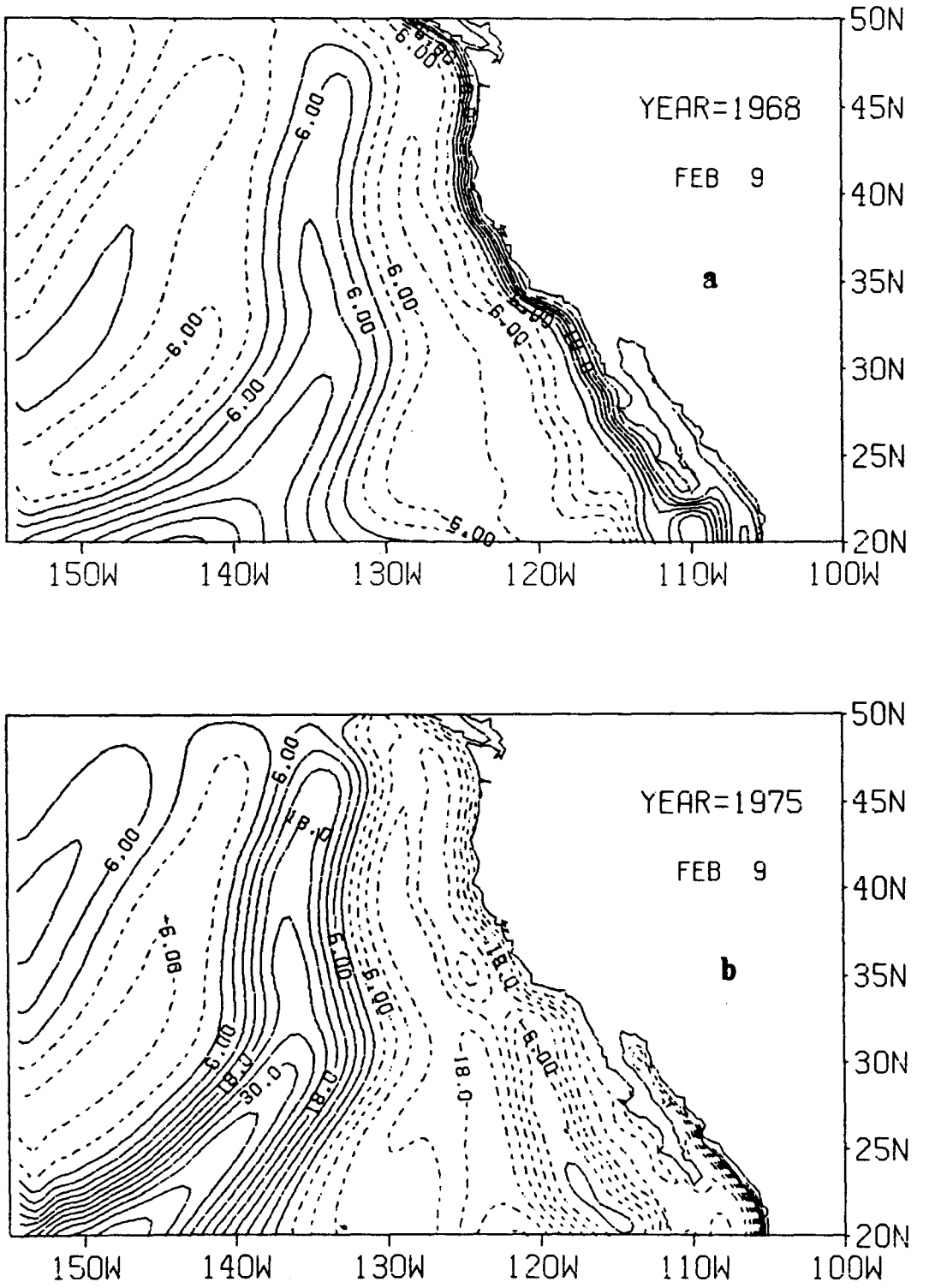

Fig. 6. Typical ULT contour from the remote model: (a) Snapshot for February 9, 1968. (b) snapshot for February 9, 1975.

San Francisco and Honolulu to investigate the source of annual baroclinic long waves in the eastern north Pacific. Their study demonstrated the importance of large amplitude fluctuations of the wind curl in the vicinity of the eastern boundary as a source mechanism for Rossby wave energy. They do not rule out the possibility of some energy contribution by locally generated upwelling and/or internal Kelvin wave propagation. More recently Cummins *et al.* (1986) simulated the annual Rossby wave field over a large part of the eastern north Pacific ocean. Through numerical integration of the linearized, reduced-gravity velocity equations in spherical coordinates, they identified three domi-

nant sources of Rossby wave energy: two along the coast, previously identified by other authors (Cummins *et al.*, 1986; White and Saur, 1981), and a mid-oceanic generation region. Their model includes realistic representation of the eastern boundary geometry.

Rossby waves and critical latitude

Plane waves of the form exp[i(kx + ly + wt)], of whatever generation mechanism, eventually adopt the form of propagating Rossby waves whose frequency, in a linear reduced-gravity model, is given by the dispersion relation:

$$w = \frac{-\beta k}{k^2 + l^2 + \alpha^{-2}} \qquad (1)$$

where α is the internal radius of deformation

$$\left(\alpha = \frac{\sqrt{g'H}}{f}\right)$$

In terms of k (the zonal wave number), and neglecting the meridional wavenumber l, eq. 1 becomes

$$k = \frac{-\beta}{2\omega}\left[1 \pm \sqrt{1 - \frac{4\omega^2}{\alpha^2 \beta^2}}\right] \qquad (2)$$

which shows that a critical latitude exists, defined as:

$$\theta_c = \tan^{-1}\left[\frac{(g'H)^{1/2}}{2a\omega}\right] \qquad (3)$$

which causes the square root in 2 to vanish. North of the critical latitude the root in eq. 2 is an imaginary term that implies a westward decaying component in the waves (McCreary *et al.*, 1987). Comparison between Figures 5 and 6 illustrates the effect of this critical latitude in the model. Figure 5 shows clearly that a critical latitude occurs near central California. The difference between the regions north and south of the critical latitude is striking. On the other hand, the interannual disturbance (Figure 6) is not similarly confined to the south of a critical latitude. Both results are in agreement with theory. The difference, as stated above, is the different composition in terms of the dominant frequencies. While the wind-driven model is dominated by the annual frequency, whose critical latitude happens to be in the middle of this model domain, the equatorially forced variability is mostly dominated by the interannual variability (El Niño, i.e. 3-4 years) whose critical latitude falls outside the northern boundary of the model. This reinforces the notion of the El Niño phenomenon being an interannual process, though the event itself seems to last about one year, and that the information is transported by a series of fast equatorial and coastal Kelvin wave pulses. The ocean "processes" these pulses as if they were a single long interannual disturbance.

For most of the domain, where the zonal wave number is much smaller than the inverse of the radius of deformation, eq. (1) can be approximated by the long-wave linear relation between ω and k:

$$C_{px} = \frac{\omega}{k} = \frac{\beta(g'H)}{f^2} \qquad (4)$$

where both the phase velocity (C_{px}) and the group velocity are westward. By means of this zonally propagating mechanism, upwelling regions (in fact, all disturbances originated at the coast) are not necessarily confined to a radius of deformation from the coast but can propagate and contribute to the ocean interior variability.

Killworth (1979) showed that the main effect of nonlinearity on east-west propagation is through variations in the depth of the layers. A negative wind curl, for example, increases ULT through Ekman pumping so that the phase speed is larger than in the linear case. The main effect of an east-west pressure gradient is through the established Sverdrup balance. Waves slow down or speed up as they travel westward, depending on the increase or decrease of the surrounding mean ULT. In our model, this implies an increase in the propagation speed for waves generated south of about 40°N where the east-west averaged pressure gradient is negative.

Longitude-time sections

Westward propagation of remotely forced coastal variability is evident in the longitude-time plots of ULT displayed in Figure 7. The remotely forced model was sampled longitudinally at latitudes 24°, 33°, 38° and 43°N. The values of ULT were averaged in space (1/2 degrees) and in time (1 month). To avoid the zone of high variability and different dynamics near the coast (i.e., coastally propagating waves and events constrained to a radius of deformation from the boundary), the data for the longitude-time plots were extracted starting 3 degrees away from the coast. The period shown (1969-1974) was chosen to emphasize the interannual variation of the data by including the extreme 1969 and 1972 events.

Waves emanating from the coast into the interior are shown in Figure 7. The velocity of propagation indicated by the slope of the contours decreases to the north in accordance with eq. (4). Approximate velocities of propagation from Figure 7 are 1.0, .61, .46 and .37 deg/month for latitudes 24°, 33°, 38° and 43°N respectively. These velocities are to be compared with those calculated from eq. (4). Using the averaged ULT for each latitude, $\beta = 2 \times 10^{-11}$ $m^{-1}s^{-1}$, and $g' = .03$ ms^{-2} the following velocities are obtained: .95, .57, .47, and .41 deg/month for 24°, 33°, 38° and 43°N respectively. The distance which a disturbance travels decreases to the north; this is a reflection of the fact that, for a given frequency, the offshore decaying factor increases to the north. Also, the fact that the waves travel at a slower speed probably allows for more time for dissipation to take effect.

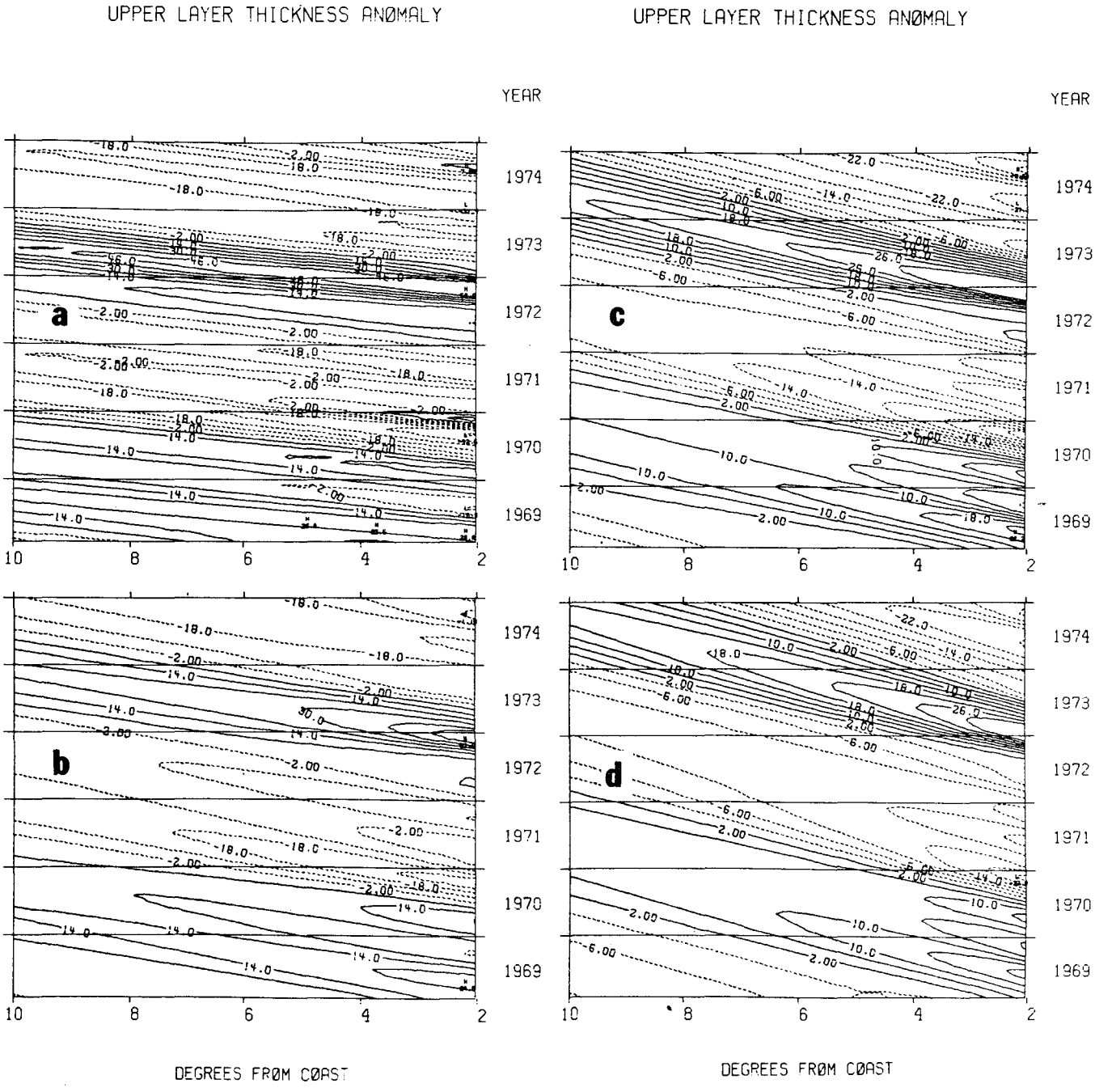

Fig. 7. Longitude-time plots of ULT from the remote model at (a) 24°N, (b) 33°N, (c) 38°N and (d) 43°N. Values in meters. Contour intervals are 8 m for (a) and (b) and 4 m for (c) and (d).

Although it is possible to distinguish (visually) an annual signal in the data, it seems that the dominant energy is at lower frequencies. This is in contrast to the strong energy at the semiannual and annual frequency found at the coast (Figure 4). The westward propagation process filters out most of the high frequency waves. While the frequency distribution of the energy at the coast for the remote model is predominantly low-frequency, the local model spectrum is dominated by the annual frequency (Figure 4). Thus even if the two mechanisms were generating an equal amount of

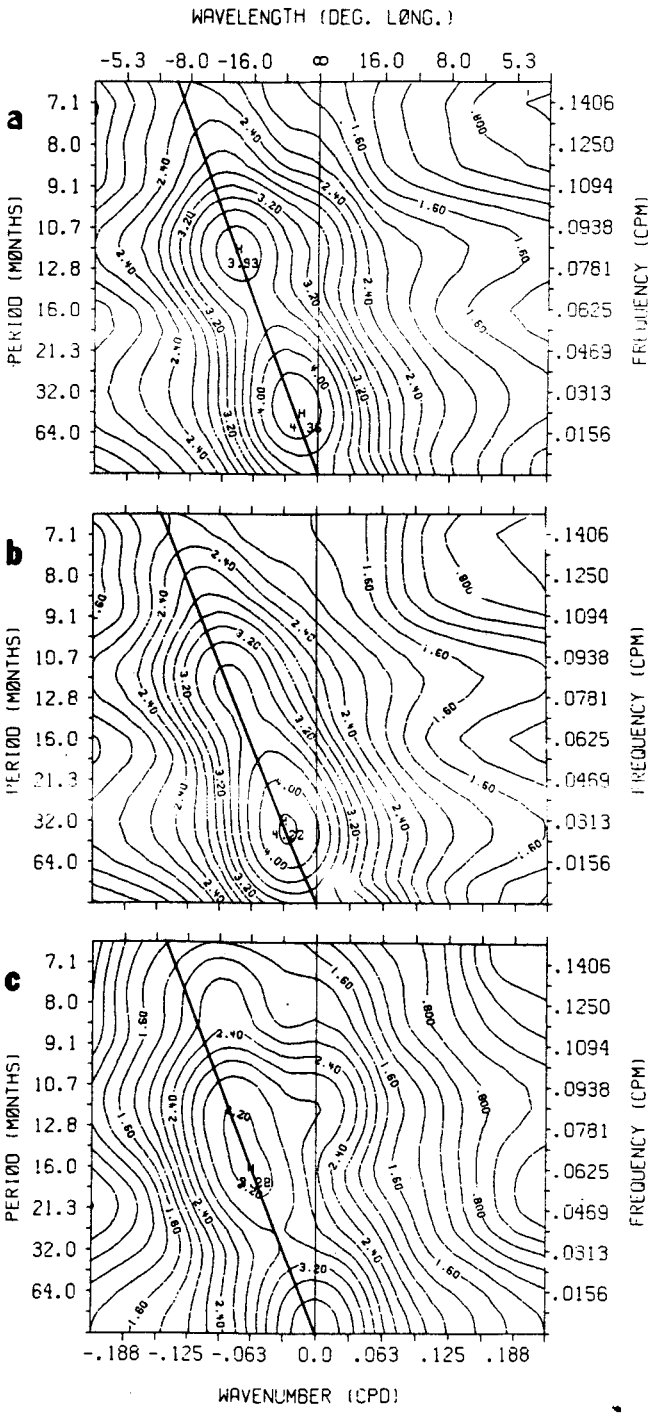

Fig. 8. Frequency-wavenumber spectra (FWS) for transect at 24°N. (a) From local + remote model, (b) from remote model and (c) from local model. The theoretical Rossby wave dispersion curve from each model is shown. The average ULT for each curve was used to calculate the theoretical dispersion curves.

total energy, most of the energy propagated westward would be of equatorial origin, north of the critical latitude of the annual frequency. It acts as a low-pass filter, where the equatorial contribution is much larger than the local.

All the information in Figures 6 and 7 originates in a 15° band in the south-eastern boundary of our model. In the light of this result, it is concluded that energy from the equatorially generated variability does reach the mid-latitude central Pacific Ocean (for a different view, see Simpson, 1984). In the present model (which is believed to extrapolate to some extent the real ocean) this part provides by far the dominant contribution to the low-frequency variability of the North Pacific.

Wavenumber-frequency Spectra

Wavenumber-frequency spectra (WFS) of ULT for the three model forcings are presented in Figures 8-11. The spectra were constructed from longitude-time matrices like those shown in Figure 7 (i.e. at latitudes 24°, 33°, 38° and 43°N), after normalization by root mean square. Due to lateral friction, the amplitude of the disturbances decreases as they propagate westward; normalization is needed to eliminate spatial changes in the variance, prior to computing the WFS (White and Tabata, 1986). Figures show the logarithm of WFS at latitude 24°N for the local + remote, remote and local models. Similarly, Figures 9, 10, 11 are the WFS for latitudes 33°, 38° and 43°N respectively. To avoid spurious contributions from the initially unforced north-western region, only the last 15 years of integration were used. Two-dimensional FFT and Hanning smoothing in frequency were used to calculate the spectrum estimates. On each WFS plot, the theoretical Rossby wave dispersion curve (eq. 4) for the corresponding latitude and averaged ULT was highlighted.

At all latitudes and for the three models, the WFS is dominated by a low-frequency-small-wavenumber band contribution and a distinctive, smaller peak at the annual frequency. The relative importance of the contribution from each of the two main frequency bands changes with latitude and from model to model. At latitude 24°N, for example, the local + remote model shows two distinctive peaks (Figure 8): one at the low frequency-small wavenumber range (64 - 25 month: ∞ - 16 degrees) that can be identified with El Niño activity, and one around the annual frequency (10 - 14 months: 16-9 degrees).

From the WFS plots, most of the ocean-interior response is in the form of westward (negative wavenumber) propagating Rossby waves. The spectral maximum energy occurs mostly along the Rossby wave dispersion curve. For example, at latitude 24°N (Figure 8), the annual peak has an associated wavelength of 11-16 degrees of longitude, while for the same model at latitude 38°N (Figure 10) the annual peak is shifted in the negative wavenumber direction to a corresponding 5 to 6 degrees wavelength. These values yield an approximate wave speed of about 12.8 degrees/year and 5.8 degrees/year at 24°N and 38°N, respectively. The pattern of maximum energy along the Rossby wave dispersion curve is common to the three models. In conclusion, once a disturbance is generated at a given latitude, either by coastally propagating waves (remote model) or by wind stress curl at the boundary (local model), at

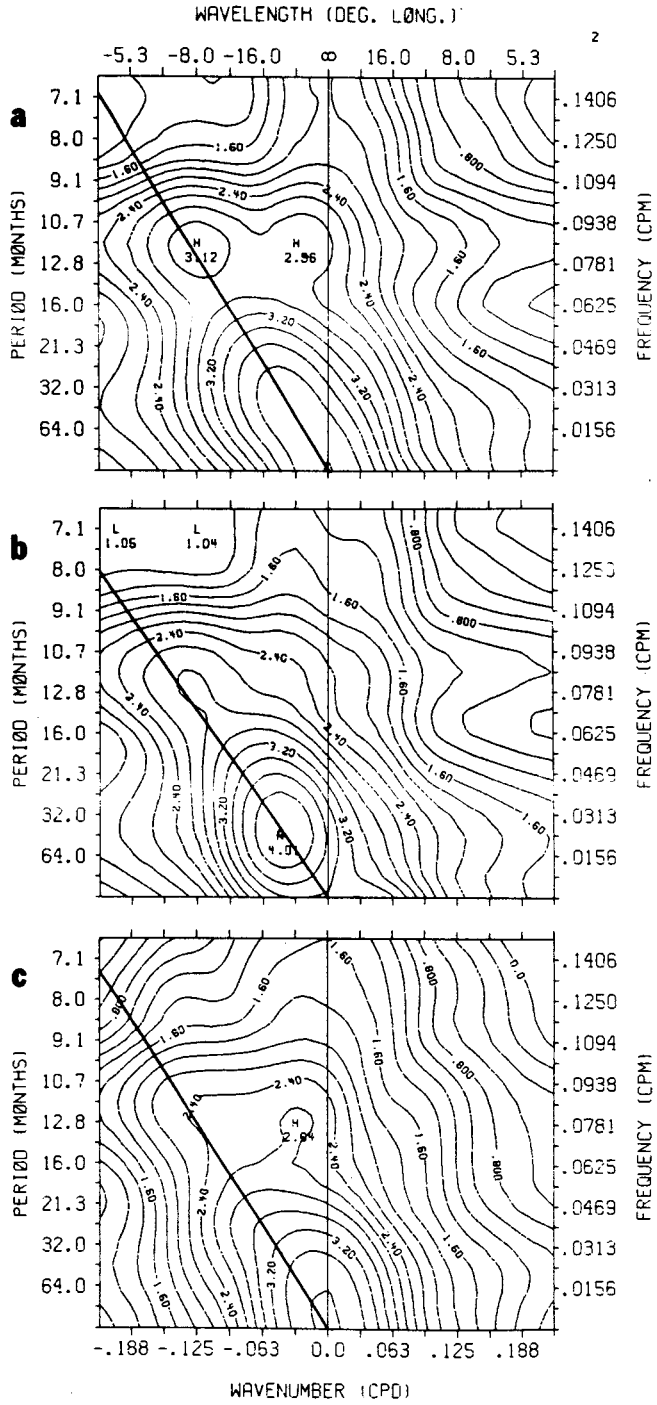

Fig. 9. As in Figure 8 but for transect at 33°N.

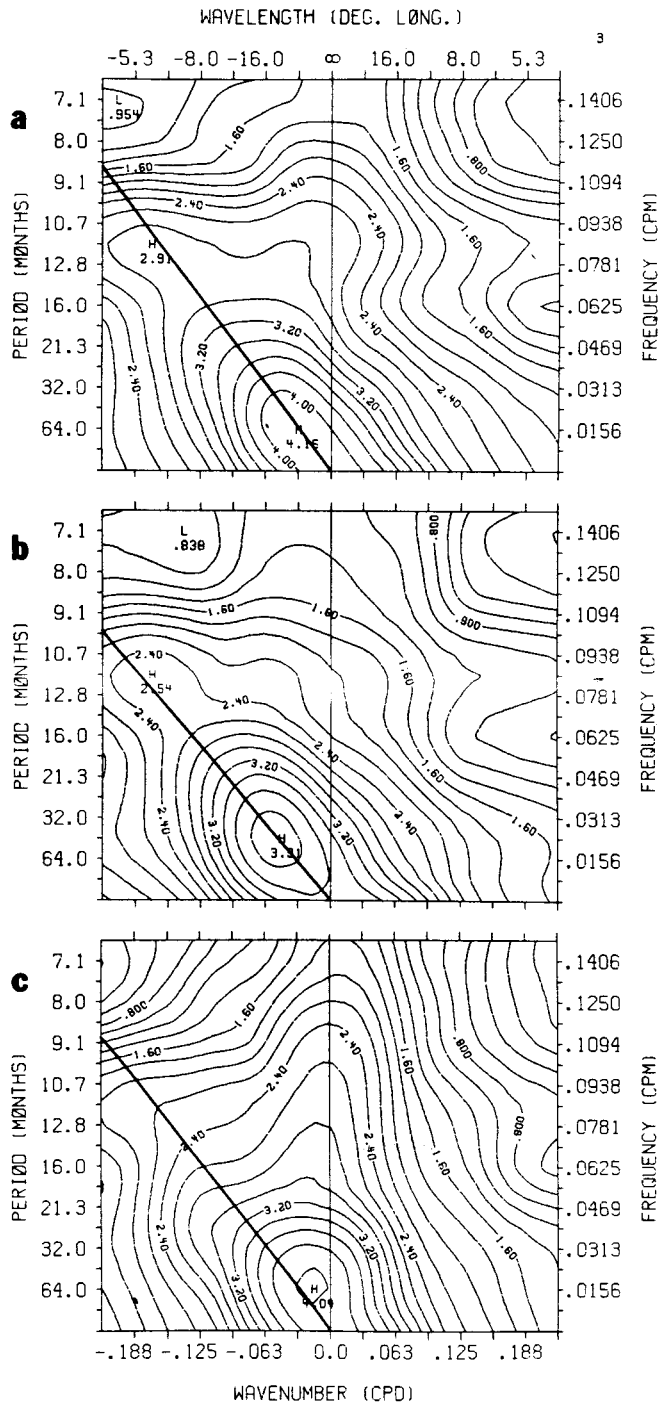

Fig. 10. As in Figure 8 but for transect at 38°N.

least some of its energy is propagated to the model interior in the form of Rossby waves.

A conspicuous exception is the peak at the annual frequency at a wavelength longer than that dictated by Rossby wave dynamics. This peak is more evident at 33°N (Figure 9), but it is also present at 38°N and 43°N (Figures 10-11). At 24°N it becomes indistinguishable from the Rossby wave annual peak. Variability at this frequency wavenumber range is most probably imposed directly by the local wind stress curl. The very small wavenumber indicates a large-scale phenomenon in the longitudinal sense; since it is present at all latitudes, it may be the result of a global annual variation in the wind forcing. Price and Magaard (1980) reported the presence of large in-phase fluctuations in broad areas of the North Pacific. For the

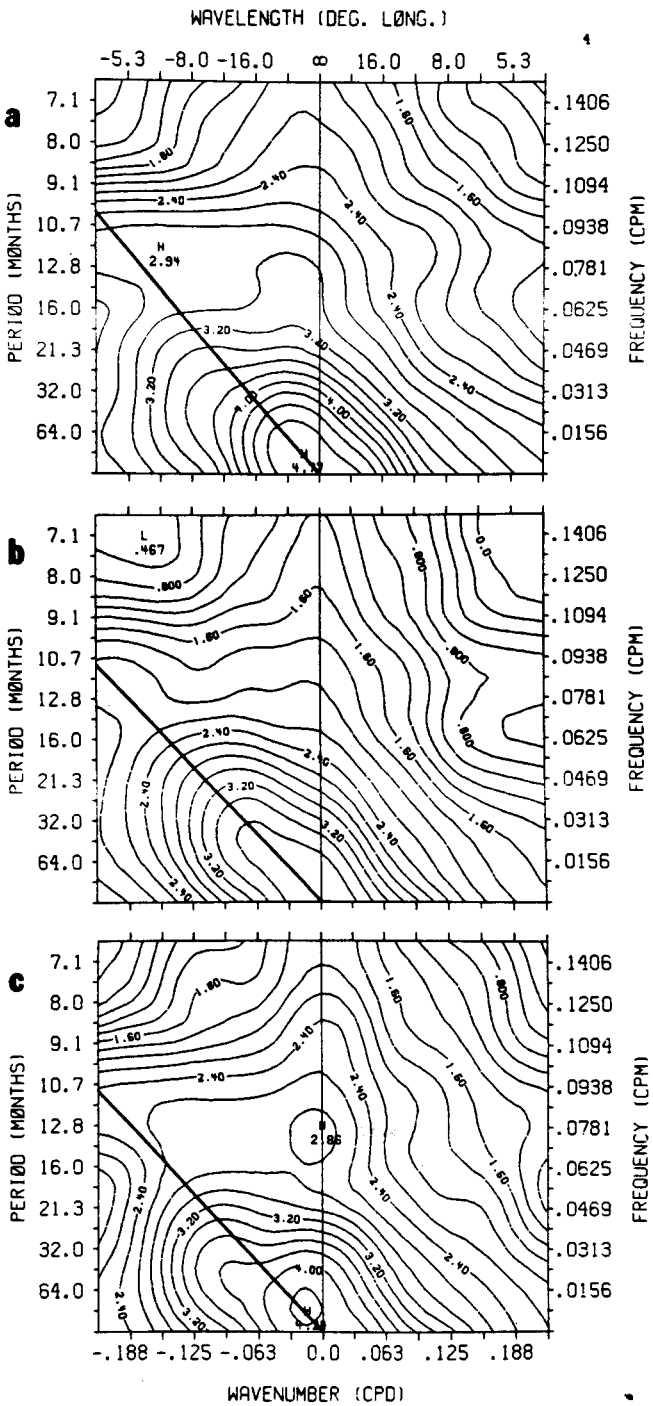

Fig. 11. As in Figure 8 but for transect at 43°N.

33° and 43°N sections it appears from the WFS plots that the contribution to the secondary annual peak (non-Rossby wave) is due to the local model.

Summary and Conclusions

A simple reduced-gravity model of the North Pacific was used to analyze the presence and sources of baroclinic low-frequency energy in the mid-Pacific Ocean. Three forcings were implemented. First, COADS winds were used to force the model in the period from 1961 to 1979. To investigate the equatorial contribution to the total mid-ocean energy, a wind forced reduced-gravity equatorial model was used. This was done by imposing at each time step the equatorial model results at our southern boundary (Figure 1). Finally the two forcings were also used simultaneously.

By comparing model outputs with observations it was found that the model reproduces to a good degree the long-term mean and long-term monthly mean ULT field in the North Pacific. Visual comparison showed the model WFS shapes to agree with those calculated from observations (e.g. White, 1985).

At all latitudes and for all three models, the WFS is dominated by a low frequency-small wave number band (64-25 months, ∞ - 16 degrees) that can be related to El Niño activity. A smaller peak at the annual period is also present. Comparison of the position of the maximum energy to the theoretical dispersion curve of first baroclinic Rosssby waves shows that most of the model's mid-ocean variability at low frequencies can be explained in terms of Rossby wave dynamics. The pattern of maximum energy along the Rossby wave dispersion curve is common to the three models: once a disturbance is generated at the coast by either mechanism, at least some of its energy leaks to the ocean interior in the form of Rossby waves.

By decomposing the total energy into a contribution of the wind forcing and a remote contribution from the variability emanated from the coast, of equatorial origin, it was found that in terms of energy both mechanisms are important. The significance of including the equatorial contribution in the model cannot be overemphasized. The amount of energy in the low frequencies at the coast contributed from the remote model is much larger than that contributed by the local model (Figure 5 and PO). Since it is in this band that the energy mostly radiates off-shore (north of about 30°N), it is concluded that the most important contribution to the low-frequency variability in the north-eastern Pacific may be of equatorial origin. The occurrence of a critical latitude for the wind forced model can be seen clearly (Figure 5). Two regions: south (off-shore propagating) and north (off-shore decaying) are separated by this latitude. Equally interesting is the lack of a critical latitude for the remotely forced variability, dominated by the El Niño signal (Figure 6).

The WFS demonstrate, first, the Rossby wave nature of the propagation and secondly, the relative composition of the low frequency compared with the annual frequency in each of the experiments and how they change with latitude. However, due to the normalization of the WSF it is not possible to compare sources directly. A more detailed analysis is required in order to quantify the contributions of each.

ACKNOWLEDGMENTS

This work was supported by Office of Naval Research grant ONR N00014-915-1278. Additional support was provided by the Consejo Nacional de Ciencia y Tecnología of México. Thanks are expressed to J. O. Brien, G. Vallis, W. White and E. Pavía for helpful comments and suggestions.

BIBLIOGRAPHY

CANE, M. A. and E. S. SARACHIK, 1977. Forced baroclinic ocean motions: II. The linear equatorial bounded case. *J. Mar. Res., 35*, 395-432.

CUMMINS, P. F., L. A. MYSAK and K. HAMILTON, 1986. Generations of annual Rossby waves in the North Pacific by the wind stress curl. *J. Phys. Oceanog., 16*, 1979-2189.

EMERY, W. J. and L. MAGAARD, 1976. Baroclinic Rossby waves as inferred from temperature in the eastern Pacific. *J. Mar. Res.*, 34, 365-385.

GRIMSHAW, R. and J. S. ALLEN, 1988. Low-frequency baroclinic waves off coastal boundaries. *J. Phys. Oceanog., 18*, 1124-1143.

HICKEY, B. M., 1979. The California current system - hypothesis and facts. *Progress in Oceanog., 8*, 279 pp.

JOHNSON, M. A. and J. J. O'BRIEN, 1990. The role of coastal Kelvin waves on the northeast Pacific Ocean. *J. Mar. Systems, 1*, 29-38.

KILLWORTH, P. D., 1979. On the propagation of stable baroclinic Rossby waves through a mean shear flow. *Deep-Sea Res., 26A*, 997-1031.

KUBOTA, M. and J. J. O'BRIEN, 1988. Variability of the upper tropical Pacific ocean model. *J. Geophys. Res., 93*, 13930-13940.

LYNN, R. J. and J. J. SIMPSON, 1987. The California Current System: The seasonal variability of its physical characteristics. *J. Geophys. Res.,92*, 12947-12966.

McCREARY, J., 1976. Eastern tropical ocean response to changing wind stress systems: with application to El Niño. *J. Phys. Oceanog., 6*, 632-649.

McCREARY, J. P. and P. K. KUNDU, 1985. Western boundary circulation driven by an alongshore wind: With application to the Somali Current System. *J. Mar. Res., 43*, 493-516.

McCREARY, J. P., P. K. KUNDU and S. CHAO, 1987. On the dynamics of the California Current System. *J. Mar. Res., 45*, 1-32.

MYSAK, L. A., 1983. Generation of annual Rossby waves in the North Pacific. *J. Phys. Oceanog., 13*, 1908-1923.

NELSON, C. S., 1977. Wind stress and wind stress curl over the California current,. NOAA Technical Report NMFS SSRF-714, U. S. Department of Commerce.

PARES-SIERRA, A. and J. J. O'BRIEN, 1989. The seasonal and interannual variability of the California Current system: A numerical model. *J. Geophys. Res., 94*, 3159-3180.

PRICE, J. M. and L. MAGAARD, 1980. Rossby wave analyses of barotropic potential energy in the upper 500 m of the North Pacific. *J. Mar. Res., 38*, 249-264.

SHRIVER, J. F., M. A. JOHNSON and J. J. O'BRIEN, 1991. Analysis of remotely forced Rossby waves off California. *J. Geophys. Res., 96*, 749-757.

SIMPSON, J. J., 1984. El Niño-induced onshore transport in the California Current during 1982-1983. *Geophys. Res. Lett., 11*, 241-242.

WHITE, W. B., 1985. The resonant response of interannual baroclinic Rossby waves to wind forcing in the eastern midlatitude North Pacific. *J. Phys. Oceanog., 15*, 403-415.

WHITE, W. B. and J. F. T. SAUR, 1981. A source of annual baroclinic waves in the eastern subtropical North Pacific. *J. Phys. Oceanog., 11*, 1452-1462.

WHITE, W. B. and J. F. T. SAUR, 1983. Sources of interannual baroclinic waves in the eastern subtropical North Pacific. *J. Phys. Oceanog., 13*, 532-544.

WHITE, W. B. and S. TABATA, 1987. Interannual westward-propagating baroclinic longwave activity on line P in the eastern midlatitude North Pacific. *J. Phys. Oceanog., 17*, 385-396.

A. Parés-Sierra
Scripps Institution of Oceanography, La Jolla CA, 92093 USA and Centro de Investigación y Estudios Superiores de Ensenada, Apdo. postal 2732, Ensenada, B.C. 22830, México.